Study of Induced EHD Flow by Microplasma Vortex Generator

メタデータ	言語: eng
	出版者:
	公開日: 2020-02-14
	キーワード (Ja):
	キーワード (En):
	作成者: Blajan, Marius, Nonaka, Daisuke, Kristof, Jaroslav, Shimizu, Kazuo
	メールアドレス:
	所属:
URL	http://hdl.handle.net/10297/00027058

Study of Induced EHD Flow by Microplasma Vortex Generator

Marius Blajan, Daisuke Nonaka, Jaroslav Kristof, and Kazuo Shimizu, *Senior Member, IEEE*

Abstract— For flow control, plasma actuators have the advantages of no moving parts. An experimental study was carried out to generate vortexes using a microplasma actuator. Also, a 3-D numerical simulation code was developed to calculate the flow generated by the microplasma actuator. The numerical simulation used the Suzen–Huang model coupled with Navier–Stokes equations. Our microplasma actuator has a thin dielectric layer with a thickness of 25 μm between the grounded and high-voltage energized electrodes, which enables to drive our device at less than 1 kV. The high-voltage and grounded electrodes have both holes. In the series of experiments, an ac voltage with an amplitude 1 kV and a frequency of 20 kHz was applied to the electrode. The induced flow was visualized using an Nd: YVO$_4$ 532-nm laser, and the flow velocity was measured using the particle tracking velocimetry (PTV) method. Incense smoke was utilized as a tracer particle. The electrohydrodynamic (EHD) flow was induced around the holes of high-voltage electrode, thus vortexes appeared above these holes. In order to study the basic phenomena of the flow, one and four holes were isolated from the electrode; thus, the phenomena could be observed in a simplified version of the electrode. The 3-D numerical simulation code showed similar results both in values and flow configuration compared with the experimental results.

Index Terms— Electrohydrodynamic (EHD) flow, microplasma, numerical simulation.

I. INTRODUCTION

THE conventional actuators used on aircraft could be replaced with plasma actuators that are a safe and efficient alternative due to their lack of moving parts, simple construction, and fast response due to the electric field. The dielectric barrier discharge (DBD) plasma actuators developed by various researchers are conventionally energized at voltages of tens of kilovolts [1]–[6]. Such high voltages are difficult to insulate and require a large-sized power supply. For flow control applications, we have developed a microplasma vortex generator that can be energized at only 1 kV.

The electrohydrodynamic (EHD) phenomenon occurs through the momentum transfer from ions accelerated by an electric field to neutral molecules by collision [1]–[5]. This can be achieved using DBD or corona discharge. In the case of high-speed flow control, corona discharge was used [6]–[14]. Turbulent boundary layer separation control, steady airfoil leading-edge separation control, oscillating airfoils dynamic stall control, and circular cylinder wake control are applications of particular flow control [15]–[20]. The microsized plasma actuator could be used for surface flow modification, such as separation flow control or drag reduction [21]–[24].

Microplasma is a type of DBD nonthermal plasma that proved to be a more economical and ecological replacement of conventional technologies for surface treatment of various materials, indoor air treatment, biomedical applications, or flow control [25]–[29].

In microplasma actuators, because of the small dimensions, it is difficult to obtain experimental observations and measurements. In this study, numerical simulations were carried out in order to investigate the flow velocity near the electrode surface where the experimental measurements were difficult to carry out.

The numerical simulation of the flow modification was carried out using the Suzen–Huang model [30], [31]. The model considers the electric potential of the plasma actuator as the combination of the potential of the external electric field and the potential of charge density of the plasma. Thus, the resultant potential can be calculated and furthermore the body-force. In the Navier–Stokes equations, the body force is introduced as forcing term in order to obtain the flow [30]–[32]. The most common models for the numerical simulations of plasma actuators are the plasma fluid model and the particle-in-cell model [33]–[42]. The Suzen–Huang model is close to the physical phenomena of the plasma actuator and was also used by other researchers [38]–[40].

Our first approach in modeling the microplasma actuator consisted of a simulation code based on the Suzen–Huang model for 2-D flow [43].

The study carried out in this article is still a fundamental one, and possible applications of this vortex generator could be drag reduction. The aim of this article is to investigate the fundamental phenomena of microplasma vortex generator and validate a numerical simulation code.

II. EXPERIMENTAL SETUP

Despite the requirement of low discharge voltage, the microscale plasma actuator has the advantage of easy integration due to its small size. Fig. 1 shows images and the schematic of the DBD microplasma actuator vortex generator. A perforated plate (topside electrode) is placed above a

This article has been accepted for inclusion in a future issue of this journal. Content is final as presented, with the exception of pagination.

2   IEEE TRANSACTIONS ON PLASMA SCIENCE
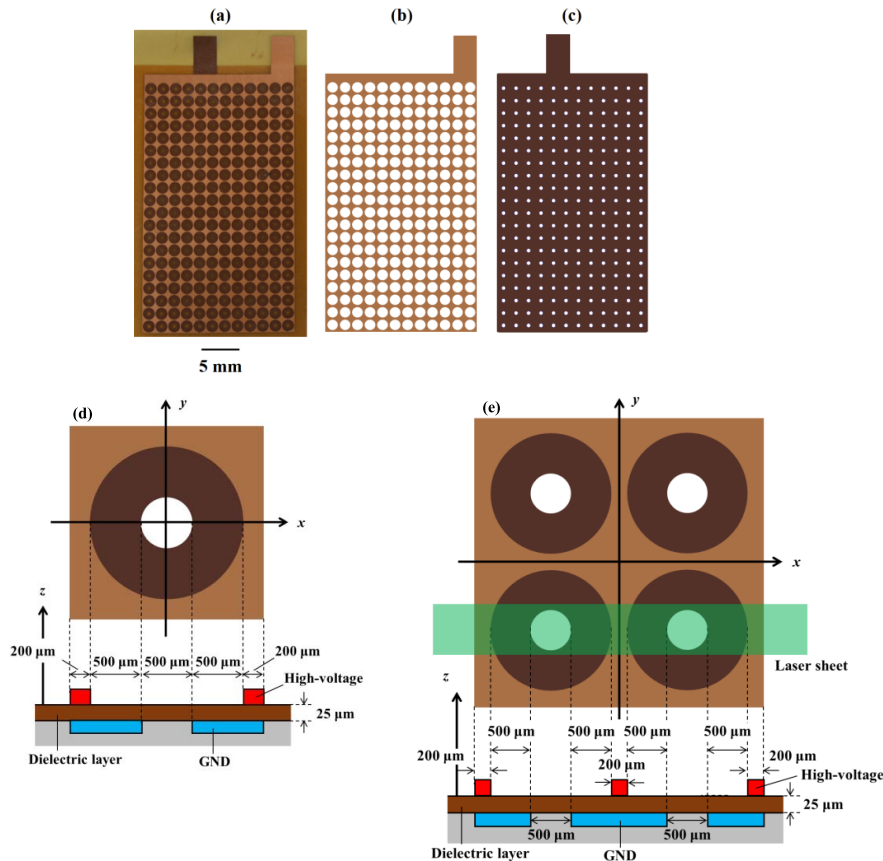

Fig. 1.   Microplasma vortex generator. (a) Image of microplasma vortex generator. (b) Image of the topside electrode. (c) Image of the bottom-side electrode. (d) Schematic of the one-hole measurement setup. (e) Schematic of four-hole measurement setup.

perforated plate electrode (bottom-side electrode) having a 25-μm-thick dielectric layer between them, as shown in Fig. 1(a)–(c). The holes size for the topside electrode was 1.5 mm, and for the bottom side, it is 0.5 mm.

Due to the microscale gap, a high electric field ($10^7 \sim 10^8$ V/m) could be obtained at the topside electrode by application of a voltage of 1 kV. Such a low voltage is easy to insulate or control and contributes to the miniaturization of the system.

In order to study the basic phenomena of the flow, one and four holes were isolated from the electrode; thus, the phenomena could be observed in a simplified version of the electrode, as shown in Fig. 1(d) and (e).

The flow was visualized by using the particle tracking velocimetry (PTV) [44]. Approximately, 0.3-μm tracer particles were used as incense smoke. The Nd YVO4 532-nm laser was utilized to visualize the flow. The experimental setup is shown in Fig. 2. The phenomena induced by the microplasma actuator were measured with a high-speed camera of 1280 $\times$ 128 pixel resolution. The recording frequency was set to 4000 Hz. The PTV results within the area of -2 mm $\leq x \leq 2$ mm and 0 mm $\leq z \leq 2.0$ mm with a resolution of 0.2 mm in the x- and z-axes were obtained manually using two consecutive images taken at each state. The applied ac voltage had an amplitude voltage of 1 kV and a frequency of 20 kHz.
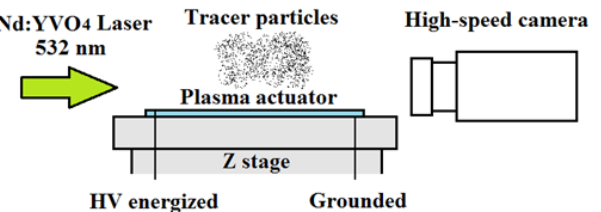

Fig. 2.   Flow velocity measurement experimental setup. Tracer particles were used to visualize the flow.

III. RESULTS

The experiments were carried out for one- and four-hole setups, and the measurement were carried out along the x-axis and z-axis and for a given value of the y-axis, as shown in Fig. 1(d) and (e).

Because of the complexity of the flow and also due to small size of microplasma vortex generator, the experiments are difficult to carry out and obtain data to characterize the flow. Thus, in order to have more information about the flow, numerical simulations were carried out.

A. Experimental Results

Experiments carried out for one-hole setup showed initial vortexes near the center of the hole at 5 ms, as shown in the images and corresponding PTV results from Fig. 3. The

This article has been accepted for inclusion in a future issue of this journal. Content is final as presented, with the exception of pagination.

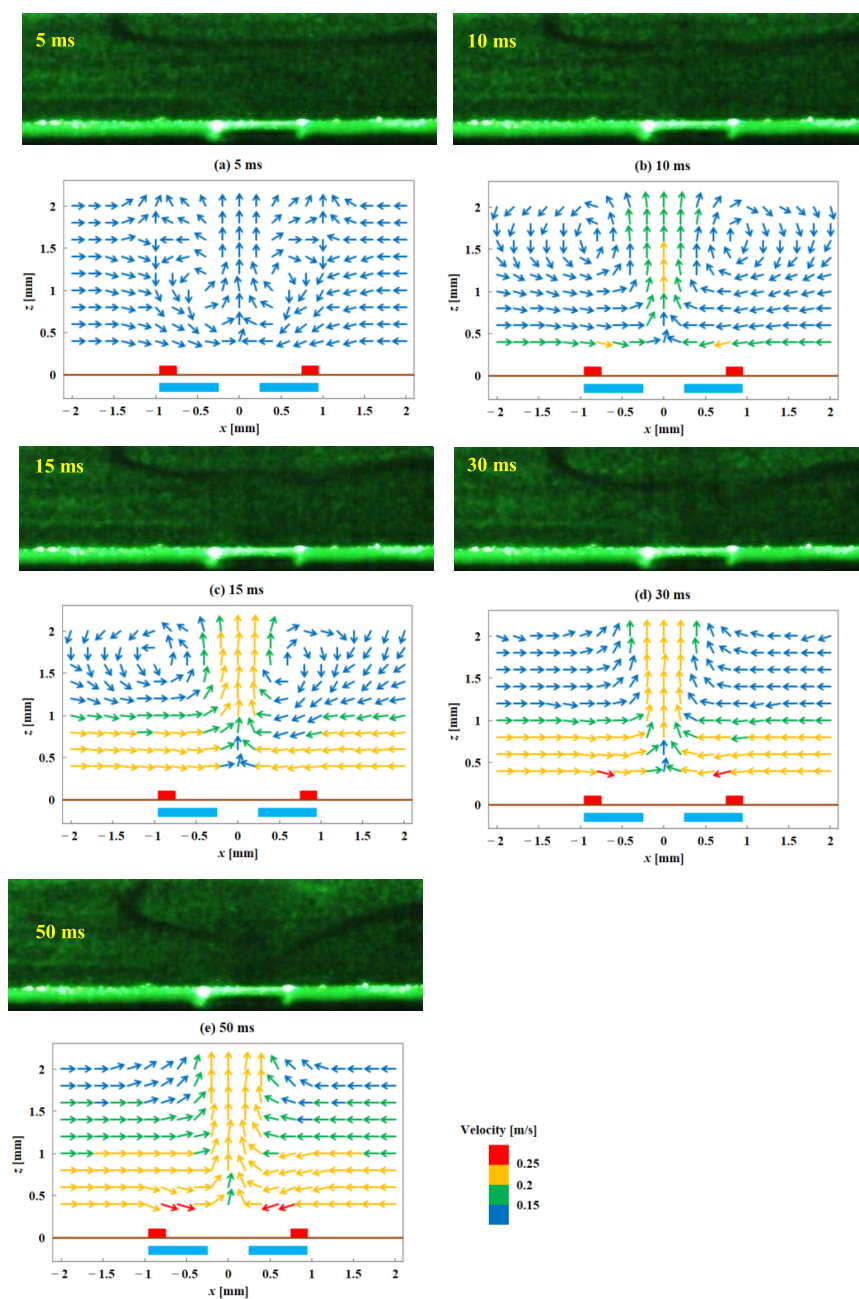BLAJAN *et al.*: STUDY OF INDUCED EHD FLOW BY MICROPLASMA VORTEX GENERATOR

3

Fig. 3.   Flow generated by one-hole setup at (a) 5, (b) 10, (c) 15, (d) 30, and (e) 50 ms. Above: actual flow. Bottom: corresponding PTV results.

measurements were carried out along the x-axis and z-axis and for y-axis value corresponding to the center of the hole. With the lapse of time to vortexes to move up and toward extremities and at 50 ms, an upward flow at the center was measured. The maximum flow velocity was about 0.3 m/s and was measured at 30 and 50 ms near the edges of the hole. Due to the geometry of the microplasma vortex generator and also because of the microplasma light emission inside the hole, the flow could not be measured. The experiments were carried out only on a single xz plane; thus, a complete image of the flow is not available. We have already studied another type of microplasma actuator that has symmetry on the y-axis [43]; thus, the flow characteristics were the same along the y-axis. Further experimental research with this type

of vortex generator will be carried out to measure the flow on various plane coordinates.

The experimental results obtained for the four-hole setup are shown in Fig. 4. The phenomena that occurred at 5 ms show vortexes above each hole and with the lapse of time smaller vortexes in the center part between the holes and bigger vortexes at the extremities at 30 and 50 ms. A higher intensity flow of about 0.3 m/s was measured at 30 and 50 ms near the edges of the holes and at more than 1.6 mm up from the center. In the center part at 50 ms up to 1.6 mm, the flow is composed of two vortexes with a flow speed of about 0.15 m/s. The vortexes have almost the same pattern from 5 to 50 ms. At more than 1.6 mm, the flow in the center is upward flow.

This article has been accepted for inclusion in a future issue of this journal. Content is final as presented, with the exception of pagination.

4   IEEE TRANSACTIONS ON PLASMA SCIENCE
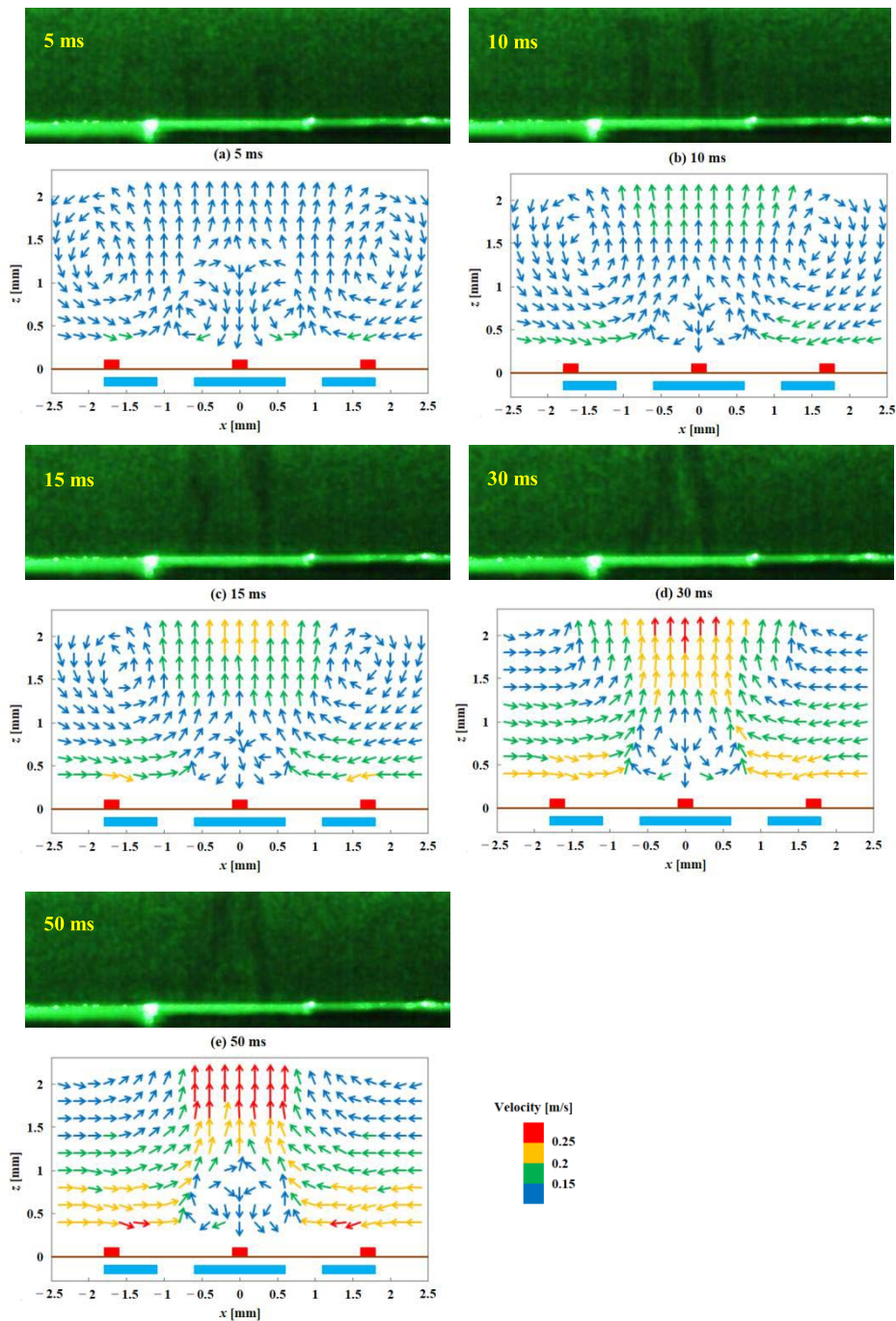

Fig. 4.   Flow generated by four-hole setup at (a) 5, (b) 10, (c) 15, (d) 30, and (e) 50 ms. Above: actual flow. Bottom: corresponding PTV results.

Comparing the one- and four-hole results, it can be observed that in the case of one-hole setup, the flow is only upward flow, but in the case of four-hole setup, also, some vortexes could be observed even after 50 ms. The flow was measured in the xz plane above two holes, but all the four holes are influencing the flow pattern. The complexity of the flow is higher than in the case of one-hole setup.

The flow could not be measured inside the holes and also above the electrodes up to about 0.2 mm; thus, numerical simulations were carried out.

B. Simulation Results

Numerical simulations could give more information about the phenomena near the active electrodes. The Suzen–Huang model [30], [31] was used for developing the simulation code. According to the model, the EHD force is given as

$$\vec{f} = \rho_c \cdot \vec{E} \tag{1}$$

where f is the body force per unit volume, ρ_c is the net charge density, and E is the intensity of the electric field.

This article has been accepted for inclusion in a future issue of this journal. Content is final as presented, with the exception of pagination.

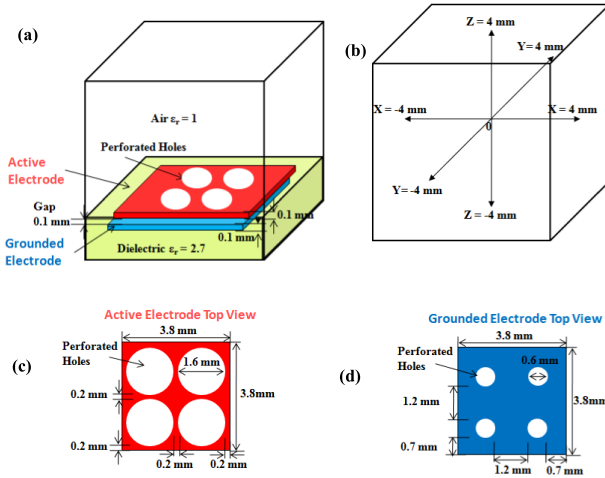BLAJAN *et al.*: STUDY OF INDUCED EHD FLOW BY MICROPLASMA VORTEX GENERATOR

5

Fig. 5. Computational geometry. (a) 3-D arrangement of the computational geometry. (b) Coordinates. (c) Top view of the active electrode. (d) Top view of the grounded electrode.

The magnetic field was not considered in calculations. The electric field is given as

$$\vec{E} = -\nabla V \tag{2}$$

where V is the potential. From Gauss' law

$$\nabla(\varepsilon \cdot \vec{E}) = \rho_c \tag{3}$$

and

$$\nabla(\varepsilon \cdot \nabla V) = -\rho_c \tag{4}$$

where ε is permittivity that was calculated as the product of relative permittivity ε_r and the permittivity of free space ε_0. The charge density considers the potential V and the Debye length λD

$$\frac{\rho_c}{\varepsilon_0} = \left(-\frac{1}{\lambda_D^2}\right) V. \tag{5}$$

From (1) and (5), the body force is calculated. Because of the atmospheric pressure microplasma and consequently weakly ionized gas particles, the potential V was considered in the Suzen–Huang model as being composed of the potential ø of the external electric field, and the potential φ potential of the net charge density

$$V = \text{ø} + \varphi. \tag{6}$$

Thus, two independent equations can be written

$$\nabla(\varepsilon_r \cdot \nabla \text{ø}) = 0 \tag{7}$$

$$\nabla(\varepsilon_r \cdot \nabla \varphi) = \frac{-\rho_c}{\varepsilon_0}. \tag{8}$$

Considering

$$\frac{\rho_c}{\varepsilon_0} = \left(-\frac{1}{\lambda_D^2}\right) \varphi \tag{9}$$

(8) will become

$$\nabla(\varepsilon_r \cdot \nabla \rho_c) = \frac{\rho_c}{\lambda_D^2}. \tag{10}$$
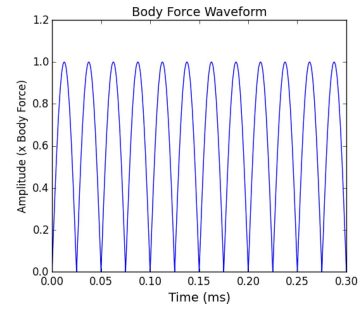

Fig. 6. Body force waveform.

Equations (7) and (10) are solved, and thus, we can calculate de body force

$$\vec{f} = \rho_c \cdot \vec{E} = \rho_c(-\nabla \text{ø}). \tag{11}$$

The harmonic mean of the permittivity of the dielectric material that covers the grounded electrodes with $\varepsilon_{rd} = 4$ and air with $\varepsilon_{rair} = 1$ was calculated for the conservation of the electric field [30]. For the potential ø, the outer boundary conditions were

$$\frac{\partial \text{ø}}{\partial x} = 0; \quad \frac{\partial \text{ø}}{\partial y} = 0; \quad \frac{\partial \text{ø}}{\partial z} = 0. \tag{12}$$

For the potential φ, the outer boundary conditions were

$$\rho_c = 0. \tag{13}$$

As written in (10), we calculated the charge distribution over electrodes covered with dielectric material by considering these electrodes as source charge. The value of the source charge in our calculations was $\rho_c = 0.0075$ C/m^3. Also, $\lambda_D = 0.00017$ m for the air, and $\lambda_D = \infty$ for the dielectric [31]. By assuming the embedded electrode as a source for the charge density, solution of (10) automatically results in a charge density distribution on the surface above the embedded electrode similar to the distribution observed in experiments, and the model does not require prescription of a charge density distribution on the surface and, thus, makes the modeling of generic actuator geometries, including generic shapes and orientations of electrodes straightforward [31]. Equation (11) was solved, and the body forces F_x, F_y, and F_z on x-, y-, and z-axes, respectively, were obtained. Furthermore, F_x, F_y, and F_z were introduced in the Navier–Stokes equations (14)–(16) in order to obtain the flow

$$\frac{\partial u}{\partial t} + u\frac{\partial u}{\partial x} + v\frac{\partial u}{\partial y} + w\frac{\partial u}{\partial z}$$
$$= \frac{-1}{\rho}\frac{\partial p}{\partial x} + v\left(\frac{\partial^2 u}{\partial x^2} + \frac{\partial^2 u}{\partial y^2} + \frac{\partial^2 u}{\partial z^2}\right) + Fx \tag{14}$$

$$\frac{\partial v}{\partial t} + u\frac{\partial v}{\partial x} + v\frac{\partial v}{\partial y} + w\frac{\partial v}{\partial z}$$
$$= \frac{-1}{\rho}\frac{\partial p}{\partial y} + v\left(\frac{\partial^2 v}{\partial x^2} + \frac{\partial^2 v}{\partial y^2} + \frac{\partial^2 v}{\partial z^2}\right) + Fy \tag{15}$$

$$\frac{\partial w}{\partial t} + u\frac{\partial w}{\partial x} + v\frac{\partial w}{\partial y} + w\frac{\partial w}{\partial z}$$
$$= \frac{-1}{\rho}\frac{\partial p}{\partial z} + v\left(\frac{\partial^2 w}{\partial x^2} + \frac{\partial^2 w}{\partial y^2} + \frac{\partial^2 w}{\partial z^2}\right) + Fz. \tag{16}$$

This article has been accepted for inclusion in a future issue of this journal. Content is final as presented, with the exception of pagination.

6   IEEE TRANSACTIONS ON PLASMA SCIENCE
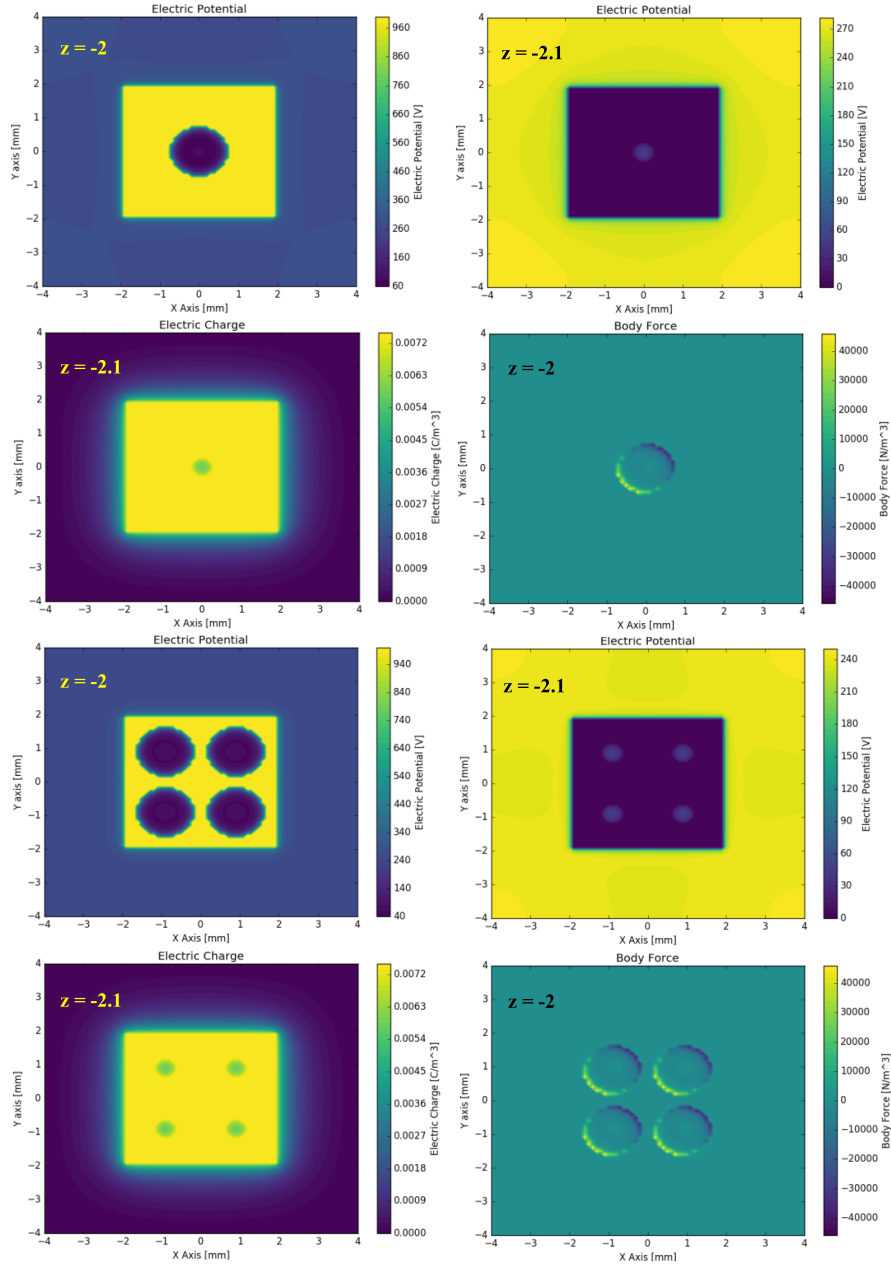

Fig. 7. Electric field, electric charge, and body force for one- and four-hole setups.

The flow velocity has the components u, v, and w on the x-, y-, and z-axes, respectively. In (14)–(16), ρ is the fluid density and v is the kinematic viscosity. We calculated the dynamic viscosity μ

$$\mu = \rho \cdot v. \tag{17}$$

Thus, taking the value of air density $\rho = 1.177$ kg/m^3 and kinematic viscosity $v = 1.57 * 10^{-5}$ m^2/s, dynamic viscosity is $\mu = 1.8 * 10^{-5}$ kg/m $\cdot$ s.

The boundary conditions were considered closed boundaries. The computational geometry is shown in Fig. 5.

The dimensions of the grid were $8 \times 8 \times 8$ mm^3 with $81 \times 81 \times 81$ grid nodes. The electrodes were centered on the xy plane; thus, the distance from the electrode edges to the limits of the computational domain on the xy plane was 2.1 mm. The electrodes were 0.1 mm in thickness and also the dielectric layer in between. For the xyz computational domain, 0 was considered in the center, as shown in Fig. 5. In the xz plane, the grounded electrode was placed from -2.2 to -2.1 mm on the z-axis. The high-voltage electrode was placed from -2 to -1.9 mm on the z-axis.

The simulation conditions were chosen to be close to the experimental one already shown in Fig. 1. The experiments were carried out by energizing the exposed electrodes with an ac waveform having amplitude 1 kV and 20 kHz. The "push–push" theory was considered in the numerical simulations; thus, the body force magnitude and direction obtained in the positive and negative half-cycles were very
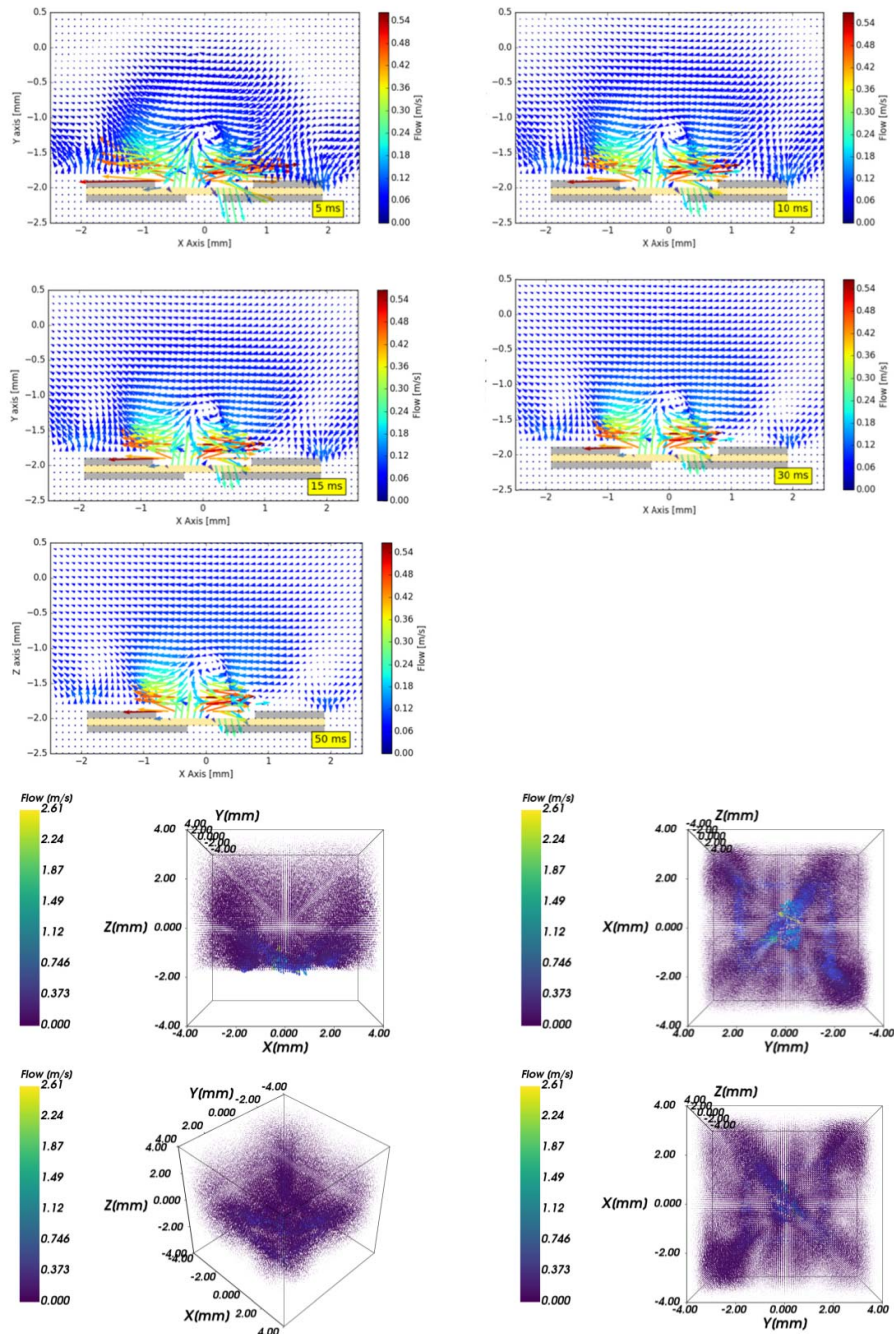
This article has been accepted for inclusion in a future issue of this journal. Content is final as presented, with the exception of pagination.

BLAJAN *et al.*: STUDY OF INDUCED EHD FLOW BY MICROPLASMA VORTEX GENERATOR

7

Fig. 8.   Flow for one-hole setup. The 2-D figures show the flow for the *xz* plane and for the *y* at 0 (center). The 3-D figures show the flow at 50 ms from various view angles.

similar [15], [32]. Therefore, for computational simplicity, we considered the double rectified sine wave as the waveform of the body force, as shown in Fig. 6.

The finite difference method was used for the discretization of the equations that were computed before solving the Navier–Stokes equations. The maximum values of the external electric field, charge, and, furthermore, body force are shown in Fig. 7. The highest intensity of body force was obtained near the edges of the holes.

The Julia programming language was used for all the simulations [45]. The Navier–Stokes equations were solved using the projection method in primitive variables on a collocated mesh. The time step was 2.5 μs.

For the one-hole setup, the flow is shown in Fig. 8. The initial stages of the phenomena are shown at 5 ms. The 2-D plots show the flow on the *xz* plane at $y = 0$. At the edges of the hole, contra-rotating vortexes form and create another vortex that results in upward flow, as shown in the experimental results. The maximum intensity of the flow in 2-D plots was about 0.54 m/s. The experimental data could be obtained starting from about 0.4 mm above the electrode, where the flow value was 0.3 m/s. In the same region,
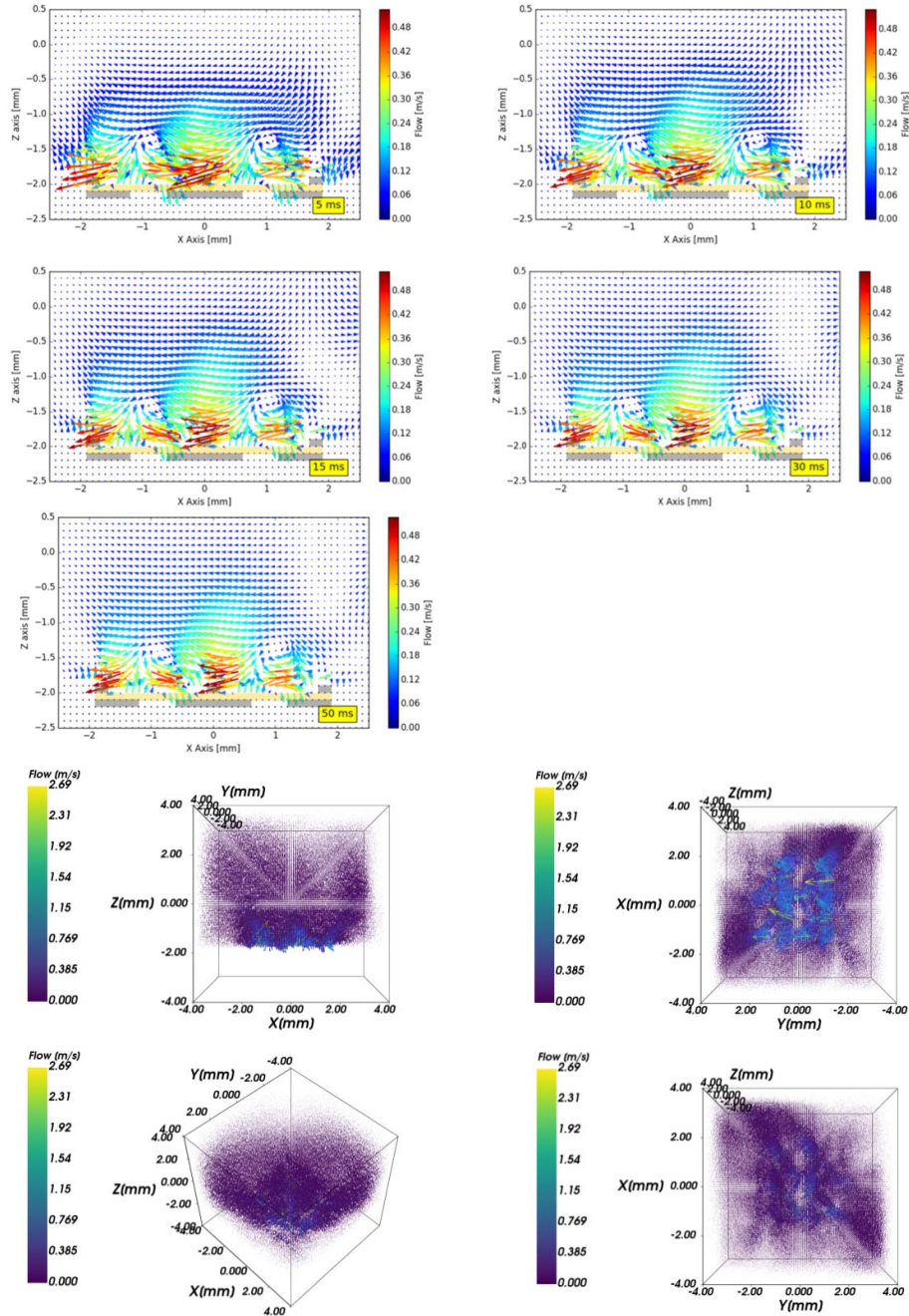
This article has been accepted for inclusion in a future issue of this journal. Content is final as presented, with the exception of pagination.

8   IEEE TRANSACTIONS ON PLASMA SCIENCE

Fig. 9. Flow for four-hole setup. The 2-D figures show the flow for the *xz* plane and for the *y* at −0.9 mm. The 3-D figures show the flow at 50 ms from various view angles.

the simulated value was 0.36 m/s. For the experimental data, the maximum value was 0.3 m/s, but the flow could not be measured inside the hole, where the flow has a higher value due to the intense plasma region.

The 3-D plots at 50 ms show a complete image of the flow generated by the one-hole setup. The highest intensity of the flow was calculated to be 2.61 m/s inside the hole and near the hole's edge. The flow shows a pattern of contra-rotating vortexes, each vortex placed above the half of the holes' edge. Because the experiments were carried out capturing the flow only in a plane on the *zx* coordinates, this phenomenon could not be observed.

The results for the four-hole setup are shown in Fig. 9. The flow shown in the 2-D plots has similar patterns with what was measured in experiments. In the experimental results shown in Fig. 4 at 50 ms, the flow has, in the center part, two vortexes with a maximum flow speed of about 0.15 m/s. Also, in Fig. 9, it can be observed two vortexes with a flow speed of about 0.2 m/s for the simulated data. A complete view of the flow is shown in the 3-D plots at 50 ms. The numerical simulation showed the complexity of the flow; because the experimental results were only obtained for a limited *xz* plane, a complete comparison between experimental and numerical simulation results will be carried out in future research.

IV. CONCLUSION

The basic phenomena of the microplasma vortex generator were studied experimentally and by numerical simulation. The following conclusions were obtained.

1) The experimental results showed, for one- and four-hole setups, a maximum flow intensity 0f 0.3 ms. For the one-hole setup, an upward flow at the center of the hole was measured considering only a 2-D xz plane. The measurements carried out for four-hole setup in a 2-D xz plane over only two holes showed vortexes in the middle part above the electrode between the holes and upward flow above the vortexes.

2) The numerical simulations showed that the flow in some parts inside the hole has 2.61 and 2.69 m/s for the one- and four-hole setups, respectively. A more complete and complex view of the flow was shown by the 3-D plots.

Future research will be carried out to experimentally investigate a more accurate 3-D representation of the flow and to fully validate the numerical simulation.

REFERENCES

[1] J. R. Roth, D. M. Sherman, and S. P. Wilkinson, "Boundary layer flow control with a one atmosphere uniform glow discharge surface plasma," in *Proc. 36th AIAA Aerosp. Sci. Meeting Exhibit*, 1998, p. 328.

[2] J. R. Roth and X. Dai, "Optimization of the aerodynamic plasma actuator as an electrohydrodynamic (EHD) electrical device," in *Proc. 44th AIAA Aerosp. Sci. Meeting Exhibit*, Jan. 2006, p. 1203.

[3] J. Jolibois, M. Forte, and E. Moreau, "Application of an AC barrier discharge actuator to control airflow separation above a NACA 0015 airfoil: Optimization of the actuation location along the chord," *J. Electrostatics*, vol. 66, pp. 496–503, Sep. 2008.

[4] N. Benard and E. Moreau, "Electrical and mechanical characteristics of surface AC dielectric barrier discharge plasma actuators applied to airflow control," *Exp. Fluids*, vol. 55, p. 1846, Nov. 2014, doi: 10.1007/s00348-014-1846-x.

[5] N. Bénard, J. Jolibois, E. Moreau, R. Sosa, G. Artana, and G. Touchard, "Aerodynamic plasma actuators: A directional micro-jet device," *Thin Solid Films*, vol. 516, no. 19, pp. 6660–6667, 2008.

[6] L. Zhao and K. Adamiak, "Electrohydrodynamic flow produced by electric corona discharge (numerical and experimental studies, and applications)," in *Proc. Electrostatics Joint Conf.*, Boston, MA, USA, Jun. 2009, pp. 1–8.

[7] D. F. Colas, A. Ferret, D. Z. Pai, D. A. Lacoste, and C. O. Laux, "Ionic wind generation by a wire-cylinder-plate corona discharge in air at atmospheric pressure," *J. Appl. Phys.*, vol. 108, no. 10, 2010, Art. no. 103306.

[8] M. Robinson, "Movement of air in the electric wind of the corona discharge," *Trans. Amer. Inst. Elect. Eng., I, Commun. Electron.*, vol. 80, no. 2, pp. 143–150, May 1961.

[9] M. S. June, J. Kribs, and K. M. Lyons, "Measuring efficiency of positive and negative ionic wind devices for comparison to fans and blowers," *J. Electrostatics*, vol. 69, no. 4, pp. 345–350, 2011.

[10] C. Kim, D. Park, K. C. Noh, and J. Hwang, "Velocity and energy conversion efficiency characteristics of ionic wind generator in a multistage configuration," *J. Electrostatics*, vol. 68, no. 1, pp. 36–41, 2010.

[11] G. Touchard, "Plasma actuators for aeronautics applications—State of art review," *Int. J. Plasma Environ. Sci. Technol.*, vol. 2, no. 1, pp. 1–25, 2008.

[12] R. D. Whalley and K.-S. Choi, "The starting vortex in quiescent air induced by dielectric-barrier-discharge plasma," *J. Fluid Mech.*, vol. 703, pp. 192–203, 2013.

[13] R. Whalley and K.-S. Choi, "Turbulent boundary layer control by DBD plasma: A spanwise travelling wave," in *Proc. 5th Flow Control Conf.*, Chicago, IL, USA, Jun./Jul. 2010, p. 4840.

[14] K.-S. Choi, T. Jukes, and R. Whaley, "Turbulent boundary-layer control with plasma actuators," *Philos. Trans. Roy. Soc. A, Math., Phys. Eng. Sci.*, vol. 369, no. 1940, pp. 1443–1458, 2011.

[15] T. C. Corke, M. L. Post, and D. M. Orlov, "Single dielectric barrier discharge plasma enhanced aerodynamics: Physics, modeling and applications," *Exp. Fluids*, vol. 46, no. 1, pp. 1–26, 2009.

[16] M. Forte, J. Jolibois, J. Pons, E. Moreau, G. Touchard, and M. Cazalens, "Optimization of a dielectric barrier discharge actuator by stationary and non-stationary measurements of the induced flow velocity: Application to airflow control," *Exp. Fluids*, vol. 43, no. 6, pp. 917–928, 2007.

[17] J. P. Boeuf and L. C. Pitchford, "Electrohydrodynamic force and aerodynamic flow acceleration in surface dielectric barrier discharge," *J. Appl. Phys.*, vol. 97, no. 10, 2005, Art. no. 103307.

[18] A. V. Likhanskii, M. N. Shneider, S. O. Macheret, and R. B. Miles, "Modeling of interaction between weakly ionized near-surface plasmas and gas flow," in *Proc. 44th AIAA Aerosp. Sci. Meeting Exhibit*, Reno, NV, USA, Jan. 2006, p. 1204.

[19] T. N. Jukes and K.-S. Choi, "Dielectric-barrier-discharge vortex generators: Characterisation and optimisation for flow separation control," *Exp. Fluids*, vol. 52, no. 2, pp. 329–345, 2012.

[20] K.-S. Choi *et al.*, "Plasma virtual actuators for flow control," *J. Flow Control, Meas. Vis.*, vol. 3, no. 1, pp. 22–34, 2015.

[21] C.-C. Wang and S. Roy, "Microscale plasma actuators for improved thrust density," *J. Appl. Phys.*, vol. 106, no. 1, 2009, Art. no. 013310.

[22] C.-C. Wang and S. Roy, "Energy and force prediction for a nanosecond pulsed dielectric barrier discharge actuator," *J. Appl. Phys.*, vol. 111, no. 10, 2012, Art. no. 103302.

[23] W. Shyy, B. Jayaraman, and A. Andersson, "Modeling of glow discharge-induced fluid dynamics," *J. Appl. Phys.*, vol. 92, no. 11, pp. 6434–6443, 2002.

[24] K. Shimizu, Y. Mizuno, and M. Blajan, "Basic study on force induction using dielectric barrier microplasma array," *Jpn. J. Appl. Phys.*, vol. 54, no. 1S, 2015, Art. no. 01AA07.

[25] K. Shimizu, T. Kuwabara, and M. Blajan, "Study on decomposition of indoor air contaminants by pulsed atmospheric microplasma," *Sensors*, vol. 12, no. 11, pp. 14525–14536, 2012.

[26] M. Blajan and K. Shimizu, "Temporal evolution of dielectric barrier discharge microplasma," *Appl. Phys. Lett.*, vol. 101, no. 10, 2012, Art. no. 104101.

[27] K. Shimizu, M. Blajan, and S. Tatematsu, "Basic study of remote disinfection and sterilization effect by using atmospheric microplasma," *IEEE Trans. Ind. Appl.*, vol. 48, no. 4, pp. 1182–1188, Jul./Aug. 2012.

[28] M. Blajan, A. Umeda, S. Muramatsu, and K. Shimizu, "Emission spectroscopy of pulsed powered microplasma for surface treatment of PEN film," *IEEE Trans. Ind. Appl.*, vol. 47, no. 3, pp. 1100–1108, May/Jun. 2011.

[29] Y. Mizuno, M. Blajan, H. Yoneda, and K. Shimizu, "Active fluid control by multi-electrode microplasma actuator," (in Japanese), *J. Inst. Electrostatics Jpn.*, vol. 39, no. 1, pp. 15–20, 2015.

[30] Y. B. Suzen, P. G. Huang, J. D. Jacob, and D. E. Ashpis, "Numerical simulations of plasma based flow control applications," in *Proc. 35th Fluid Dyn. Conf. Exhibit*, Toronto, ON, Canada, Jun. 2005, p. 4633.

[31] Y. B. Suzen, P. G. Huang, and D. E. Ashpis, "Numerical simulations of flow separation control in low-pressure turbines using plasma actuators," in *Proc. 45th AIAA Aerosp. Sci. Meeting Exhibit*, Reno, NV, USA, Jan. 2007, p. 937.

[32] D. M. Orlov, "Modelling and simulation of single dielectric barrier discharge plasma actuator," Ph.D. dissertation, Dept. Aerosp. Mech. Eng., Univ. Notre Dame, Notre Dame, IN, USA, 2006.

[33] T. Unfer and J. P. Boeuf, "Modelling of a nanosecond surface discharge actuator," *J. Phys. D: Appl. Phys.*, vol. 42, no. 19, 2009, Art. no. 194017.

[34] A. V. Likhanskii, M. N. Shneider, S. O. Macheret, and R. B. Miles, "Modeling of dielectric barrier discharge plasma actuator in air," *J. Appl. Phys.*, vol. 103, no. 5, 2008, Art. no. 053305.

[35] H. Nishida and T. Abe, "Numerical analysis for plasma dynamics in SDBD plasma actuator," in *Proc. 41st Plasmadyn. Lasers Conf.*, Jun./Jul. 2010, p. 4634.

[36] B. Jayaraman, S. Thakur, and W. Shyy, "Modeling of fluid dynamics and heat transfer induced by dielectric barrier plasma actuator," *J. Heat Transf.*, vol. 129, no. 4, pp. 517–525, 2007.

[37] G. I. Font, S. Jung, C. L. Enloe, T. E. McLaughlin, W. L. Morgan, and J. W. Baughn, "Simulation of the effects of force and heat produced by a plasma actuator on neutral flow evolution," in *Proc. 44th AIAA Aerosp. Sci. Meeting*, Jan. 2006, p. 167.

[38] I. Maden, R. Maduta, J. Kriegseis, S. Jakirlic, C. Schwarz, S. Grundmann, and C. Tropea, "Experimental and computational study of the flow induced by a plasma actuator," *Int. J. Heat Fluid Flow*, vol. 41, pp. 80–89, Jun. 2013.

[39] M. Abdollahzadeh, J. C. Páscoa, and P. J. Oliveira, "Modified split-potential model for modeling the effect of DBD plasma actuators in high altitude flow control," *Current Appl. Phys.*, vol. 14, no. 8, pp. 1160–1170, 2014.

[40] T. Brauner, S. Laizet, N. Benard, and E. Moreau, "Modelling of dielectric barrier discharge plasma actuators for direct numerical simulations," in *Proc. 8th AIAA Flow Control Conf. Aviation*, Washington, DC, USA, Jun. 2016, p. 3774.

[41] M. J. Pinheiro and A. A. Martins, "Electrical and kinetic model of an atmospheric RF device for plasma aerodynamics applications," *J. Appl. Phys.*, vol. 108, no. 3, 2010, Art. no. 033301.

[42] J. Bai, J. Sun, Q. Zhang, and D. Wang, "PIC simulation of RF hydrogen discharges in a transverse magnetic field," *Current Appl. Phys.*, vol. 11, no. 5, pp. S140–S144, 2011.

[43] K. Shimizu, Y. Mizuno, A. Ito, and M. Blajan, "Microplasma actuator for active flow control: Experiment and simulation," in *Proc. 14th Int. Conf. Global Res. Educ., Inter-Acad.*, 2016, Art. no. 011202.

[44] S. Fu, P. H. Biwole, and C. Mathis, "Particle tracking velocimetry for indoor airflow field: A review," *Building Environ.*, vol. 87, pp. 34–44, May 2015.

[45] *Julia Programming Language*. Accessed: 2017. [Online]. Available: http://julialang.org/

Daisuke Nonaka received the M.Sc. degree in electrical engineering from Shizuoka University, Hamamatsu, Japan, in 2019.

He is currently with Mitsubishi Electric, Shizuoka, Japan, where he is engaged in the design of controllers in the electronic control system section of air-conditioning equipment.

Jaroslav Kristof received the Ph.D. degree in plasma physics from Comenius University, Bratislava, Slovakia, in 2009, and the Ph.D. degree in optoelectronics and nanostructure science from Shizuoka University, Hamamatsu, Japan, in 2018.

His research at Comenius University, Bratislava, Slovakia, during years 2005–2015, included diagnostics of low-pressure plasma discharges and, in recent years, laser breakdown spectroscopy. Since 2015, his research interests include the study of plasma sources and their applications in transdermal drug delivery at Shizuoka University.

Kazuo Shimizu (S'95–M'96–SM'13) was born in Hamamatsu, Japan, in 1969. He received the B.S., M.S., and Ph.D. degrees in electrical engineering from the Toyohashi University of Technology, Toyohashi, Japan, in 1991, 1993, and 1996, respectively.

From 1996 to 2002, he was an Assistant Professor with the Graduate School of Engineering and Frontier Science, The University of Tokyo, Tokyo, Japan. He is currently an Associate Professor with the Organization for Innovation and Social Collaboration and the Graduate School of Science and Technology, Shizuoka University, Hamamatsu. His current interests are physics of microplasma and its applications, such as indoor air treatment, active flow control (plasma actuator), and biomedical application (plasma medicine).

Dr. Shimizu is also a member of the Institute of Electrical Engineers of Japan, the Institute of Electrostatics Japan, and the Japan Society of Applied Physics.

Marius Blajan received the Ph.D. degree in electrical engineering jointly from the University of Poitiers, Poitiers, France, and the Technical University of Cluj-Napoca, Cluj-Napoca, Romania, in 2006.

Since April 2008, he has been a Post-Doctoral Researcher with the Innovation and Joint Research Center, Shizuoka University, Hamamatsu, Japan. His research interests include the applications of microplasma for NO_x removal, indoor air purification, sterilization, microplasma actuators, and the study of fundamental phenomena of microplasma and electrostatics.